Tellus (1994), 46A, 598–614
Printed in Belgium – all rights reserved

TELLUS
ISSN 0280–6495

On the improvement of precipitation forecast skill from physical initialization

By T. N. KRISHNAMURTI*, G. D. ROHALY and H. S. BEDI, *Department of Meteorology, Florida State University, Tallahassee, FL 32306-3034, USA*

(Manuscript received 19 July 1993; in final form 7 January 1994)

ABSTRACT

This study explores the impact of physical initialization on the numerical weather prediction of tropical rainfall. The goal is to improve the definition of the initial state by assimilation of proposed or currently available surface and satellite-based observations during a pre-integration phase using a global spectral model. Physical initialization refers to the use of reverse algorithms consistent with the physics of the numerical model which can provide a modification of the initial state via incorporation of an analysis of tropical rainrates. This modification of the initial state variables is accomplished in an assimilation phase of the model forecast. The physical initialization process produces, in a diagnostic sense, a thermodynamic consistency between the humidity variable, the surface fluxes, rainfall distributions, diabatic heating and the clouds. A diabatic initialization is achieved by a Newtonian relaxation of the above diagnosed humidity variable where the divergent wind is permitted to evolve in response to the imposed surface fluxes and the condensation heating in a consistent manner. An important finding of this study is related to the absolute correlation of the observation only based rainfall and the model-based rainfall at the initial time and at the end of a one day forecast which are significantly improved with the use of physical initialization. The "observed" rainrates are obtained from algorithms that translate satellite-based measurements of outgoing longwave radiation and radiances for an array of microwave frequencies. In addition, the available raingauge records over the land area are incorporated to define the "observed" rainfall over the gaussian transform grid squares of a global spectral model at a high resolution (T106). Thus the rainfall measures are averages over roughly $100 \times 100\ \text{km}^2$ and 7.5 min which is the time step of the spectral model. It is for this averaged representation that we are able to demonstrate a very marked improvement in nowcasting and one day forecasts of tropical rainfall. The monthly mean rainfall climatology, thus obtained, nearly replicates the rainfall analyses provided to the physical initialization.

1. Introduction

The sparsity of conventional observations over the tropics contributes to the reduced skill in the numerical weather prediction of the low latitudes. Given the satellite-based estimates of rainrates, it is feasible to invoke a physical initialization procedure within an assimilation phase of a model forecast to enhance the information content of the initial state. The term "physical initialization" was first introduced by Krishnamurti et al. (1984) to use satellite-based rainrates thus augmenting the data content of the tropical latitudes. Specific case studies have shown the improvement in nowcasting and short range forecast skill of rainfall prediction by implementing the aforementioned procedure (Krishnamurti et al., 1991, 1993).

Currently, the satellite-based rainrates and the outgoing long wave radiaton are used to initialize the surface fluxes, the model rainrates and the model-based outgoing long wave radiation (Krishnamurti et al., 1993). The "observed rain" is defined as a mix of: algorithms based on microwave, outgoing long wave radiation and raingauge data.

* Corresponding author.

This initialization procedure includes the following five computational areas:

(a) The surface fluxes of moisture and heat are obtained from the vertical integration of the apparent moisture sink, Q_2, and the apparent heat source, Q_1, following the analysis of Yanai et al. (1973). The proposed procedure using this moisture balance relation improves these estimates as one applies it repeatedly since the divergence, heating, and the moisture fields adjust to the imposed rainrates with time. The vertical integrals of Q_1 and Q_2 are carried out from the top of the atmosphere, $\sigma = 0$, to the earth's surface, $\sigma = 1$, where σ is the vertical coordinate. (A list of acronyms is provided in Table 1 and a list of symbols is provided in Table 2).

(b) A reverse similarity theory is invoked during each time step of the physical initialization. The rainrates are assumed to be known and are used to provide the specific humidity and the potential temperature at the top of the constant flux layer. An assimilation of this data at the top of the constant flux layer promotes a consistency between the calculated fluxes and the imposed rainrate.

(c) A reverse cumulus parameterization algorithm restructures the moisture variable following the vertical coordinate which is consistent with the imposed rainrate. This restructuring of the moisture variable is achieved between the cloud base (the lifting condensation level) and the cloud top (the level at which the local moist adiabatic and the cloud-environmental sounding intersect).

Table 1. *List of acronyms*

DMSP	Defense Meteorology Space Program
FSU	Florida State University
GDAS	Global Data Assimilation System
GHz	Gigahertz
GPCP	Global Precipitation Climatology Project
IR	Infrared Radiation
NASA	National Aeronautics and Space Administration
NMC	National Meteorological Center
OLR	Outgoing Longwave Radiation
SPCZ	South Pacific Convergence Zone
SSI	Spectral Statistical Interpolation
SSM/I	Special Sensor Microwave Imager
TRMM	Tropical Rainfall Measurement Mission
UTC	Universal Time Coordinated

Table 2. *List of symbols*

E	evaporation
HH	horizontal polarization
HR	hour
mb	millibar
mm	millimeters
p	pressure
p_s	pressure at the surface
P	precipitation
Q_1	apparent heat source
Q_2	apparent moisture sink
R	rainfall rate
TB	microwave brightness temperature
T106	Triangular truncation at 106 waves
T213	Triangular truncation at 213 waves
VV	vertical polarization
Z	factor of reflectivity
σ	dimensionless vertical coordinate (p/p_s)

(d) In the upper troposphere ($\sigma < 0.5$), the moisture variable is restructured to minimize the local difference between the model and the satellite inferred fields of outgoing long wave radiation. A bisection method determines a parameter which defines the structure of the moisture variable in the upper troposphere.

(e) These components of the physical initialization are executed within a data assimilation phase of the model initialization. During this assimilation the surface fluxes, the outgoing longwave radiation, the divergence field, the diabatic heating and the surface pressure evolves in a consistent manner. The details of the above procedure are presented in the two papers Krishnamurti et al. (1991, 1993). The present study is a sequel to these two papers.

The purpose of this paper is to demonstrate the nowcasting and forecasting skill from a large number of consecutive experiments. The desire is to show the ability of the physical initialization procedure within the context of an operational environment. The Florida State University prediction system is not used for real-time forecasts, however, this large sequence of experiments provides a more realistic view of the possible advantages of physical initialization and is a more strict measure than a case by case scenario would allow. Analyses have been prepared of the daily "observed" rainfall distribution for the month of October, 1991. This rainfall was analyzed directly on to the transform grid of the global model at the horizontal resolution T106.

A comparison of two different algorithms which calculate microwave-sensed rainrates from the SSM/I instrument is also viewed within the context of this paper. This work is an extension of a previously published case study involving a triple typhoon event in the western Pacific Ocean. The Krishnamurti et al., 1993 paper forms the basis for the algorithm comparison and illustrates the power of the physical initialization to accept rainrates from diverse algorithms and provides similar skill in returning realistic rainfall at the beginning of the forecast. However, differences in medium range forecasts has strong implications on the overall quality of the rainfall analysis which is used for the initialization procedure.

2. Microwave rainrate algorithms

The acronym SSM/I refers to a special sensor microwave imager which includes 7 channels and 4 frequencies of a linearly polarized passive microwave radiometer. This instrument is on the U.S. Air Force Defense Meteorology Space Program (DMSP) spacecraft known as F8 with a circular sun synchronous orbit. Its equatorial crossing occurs during the south to north passage at 0613 local time and has an orbital period of 103 min. The SSM/I instrument includes vertically and horizontally polarized radiation sensors at 19.3, 37.0 and 85.5 GHz. The fourth frequency at 22.2 GHz only includes the capability to receive vertically polarized radiation.

It is perhaps premature to qualify the superiority of one rainrate algorithm as compared to another at the present time. Several algorithm intercomparison exercises are currently under way. In this context, we shall examine the impact on physical initialization of two such algorithms, Olson et al. (1990) and Kummerow and Giglio (1994). The Olson algorithm is multiple regression based and is described as follows:

I. For rainfall over the land

$$R = \exp(3.29716 - 0.01290 \times \mathrm{TB85VV} + 0.0087 \times \mathrm{TB85HH}) - 8.0\mathrm{MM/HR}$$

II. For rainfall over the oceans

$$R = \exp(3.06231 - 0.0056036 \times \mathrm{TB85VV} + 0.0029478 \times \mathrm{TB85HH} - 0.0018119 \times \mathrm{TB37VV} - 0.00750 \times \mathrm{TB22VV} + 0.0097550 \times \mathrm{TB19VV}) - 8.0\mathrm{MM/HR}$$

In case the 85 GHz frequency was unusable then

I. For rainfall over the land

$$R = \exp(-17.76849 - 0.09612 \times \mathrm{TB37VV} + 0.15678 \times \mathrm{TB19VV}) - 1.0\mathrm{MM/HR}$$

II. For rainfall over the oceans

$$R = \exp(5.10196 - 0.05378 \times \mathrm{TB37VV} + 0.02766 \times \mathrm{TB37HH} + 0.01373 \times \mathrm{TB19VV}) - 2.0\mathrm{MM/HR}$$

A rainrate retrieval algorithm developed by Kummerow and Giglio (1994) has been used to estimate rainrates and vertical structure information from the space-born SSM/I instrument. The SSM/I multifrequency data, in conjunction with other information relating the observed microwave brightness temperatures are required to calculate a rainrate. This is possible by focusing on the parameters which most influence the upwelling brightness temperatures.

The methodology for this retrieval algorithm is expanded upon in Kummerow et al. (1989). This approach uses a cloud radiative model to create large datasets which relate the rainrate and other geophysical parameters to the microwave brightness temperatures. From these datasets various multiple linear regression methods may be used in order to obtain regression coefficients relating the geophysical parameters to a linear combination or combinations of the observed brightness temperatures.

Recently, Kummerow and Giglio (1994) compared their algorithm to observed rainfall, ground based radar data and OLR derived rainfall at Darwin, Australia. They noted problems with the SSM/I algorithm in delineating small scale convection over land area. By excluding certain pixels over land, the IR based algorithm took precedence and resulted in a major improvement. The monthly accumulated rainfall over the Darwin area from the combined algorithm was shown to be in a reasonable agreement with the Z/R based Darwin radar estimates.

The two algorithms are similar in that the SSM/I multifrequency data, or microwave brightness temperatures, are used to calculate the observed rainrates. The difference becomes evident when considering the Kummerow–Giglio algorithm is more physically based due to its dependence upon certain relevant geophysical parameters which are generated by a cloud radiative model. However, the increased complexity in deriving the satellite-based rainrate does not imply a superiority of an algorithm as compared to one of a less complex methodology.

3. FSU global spectral model

The FSU global spectral model has been used in our earlier studies on physical initialization, Krishnamurti et al. (1991, 1993). The same model at the resolution T106 has been used to perform the experiments carried out here.

The FSU Global Spectral Model includes the following features:

(a) Independent variables: (x, y, σ, t).

(b) Dependent variables: vorticity, divergence, surface pressure, vertical velocity, temperature and dew point depression.

(c) Horizontal resolution: Triangular 106 waves.

(d) Vertical resolution: 14 layers between roughly 50 and 1000 mb.

(e) Semi-implicit time differencing scheme.

(f) Envelope orography (Wallace et al., 1983).

(g) Centered differences in the vertical for all variables except humidity which is handled by an upstream differencing scheme.

(h) 4th-order horizontal diffusion (Kanamitsu et al., 1983).

(i) Kuo-type cumulus parameterization (Kuo, 1965, 1974; Krishnamurti et al., 1983).

(j) Shallow convection (Tiedke, 1984).

(k) Dry convective adjustment.

(l) Large-scale condensation (Kanamitsu, 1975).

(m) Surface fluxes via similarity theory (Businger et al., 1971).

(n) Vertical distribution of fluxes utilizing diffusive formulation where the exchange coefficients are functions of the Richardson number (Louis, 1981).

(o) Long and shortwave radiative fluxes based on the emissivity/absorptivity methods (Chang, 1979).

(p) Diurnal cycle with respect to the radiative processes.

(q) Parameterization of low, middle and high clouds based on threshold relative humidity for radiative transfer calculations.

(r) Surface energy balance coupled to the similarity theory (Krishnamurti et al., 1988).

4. The sequence of computations

Lacking a unified column model that integrates all of the physical processes (i.e., the surface flux parameterization, the cumulus parameterization and the radiative transfer scheme), the current model has separate computational algorithms for these components. The sequence of computations within the physical initialization modifies the moisture variable separately to satisfy each requirement, i.e., fluxes, rainrate and the earth radiation budget. Fig. 1 presents a schematic out-

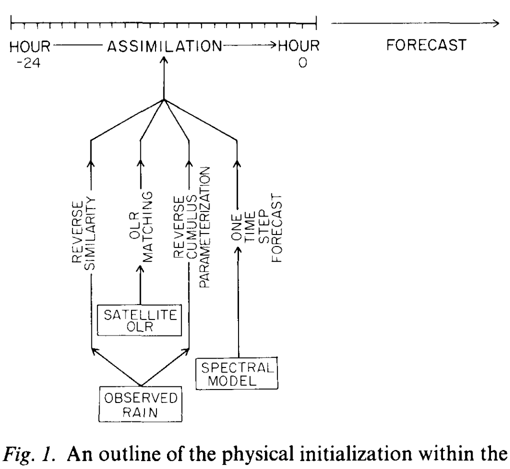

Fig. 1. An outline of the physical initialization within the assimilation phase of the global model. The package of reverse similarity, OLR matching, reverse cumulus parameterization slides from left (hour-24) to right (hour 0) during this initialization period.

line of these computations. The sequence of reverse algorithms are: reverse similarity followed by OLR matching and then the reverse cumulus parameterization. The time interpolated rainrates are an input to the reverse similarity and the reverse cumulus parameterization algorithms. The satellite-based OLR enters the matching algorithm. A one time step, forward integration follows the execution of the reverse cumulus parameterization algorithm. Since the reverse cumulus and the normal cumulus are carefully designed to be almost completely reversible, the "observed" rainrate is reproduced by the model at the end of the time step. Thus, an accumulation over 24 h of simulated assimilated rainfall appears realistic.

What is currently missed by the physical initialization are instances where the model calls for no precipitation (i.e., no net moisture convergence or absence of conditional instability) whereas the satellite or raingauge observations imply rain. We impose saturation as an upper limit for the modification of the specific humidity. This constrains the extent to which rainfall can be recovered in these instances. Further work is ongoing in both of these above areas to overcome these difficulties towards further improvement of the nowcasting skill.

5. Forecast skill from physical initialization

We shall show the results of the physical initialization and one day forecasts based on this improved initial state for a large sample of experiments. In Fig. 2 we illustrate the rainfall predictive skill in the global tropics for days 0 and 1 when the physical initialization was invoked. Also shown is the rainfall forecast skill for day 1 of control experiments where the physical initialization was not used. Results of 31 forecasts are shown; these results show a marked skill at day 0 and day 1 for the physically initialized experiments. These skills are substantially above those of the control run. The skill is measured by the absolute correlation of the 24-h rainfall totals at the transform grid squares between 29.719S and 29.719N latitudes. The observed rainfall is the 24-h rainfall total ending at day 0 or day 1 of the forecasts.

A certain amount of caution should be used in assessing an impact in rainfall prediction. If a rainfall analysis has used model output as the first guess or the rainfall analysis is from the assimilation system which is model dependent, then a comparison of interdependent data is a valid concern for a diagnosis of forecast skill. The FSU rainfall analysis is achieved in a manner which is completely independent of the model and is solely based on three different measurement techniques. Rain gauge and SSM/I observations provide a high quality rainrate data set with the sharpened outgoing long-wave radiation derived rainrates furnishing the first-guess for the analysis scheme (Gairola and Krishnamurti, 1992).

Perhaps the most spectacular result is the nowcasting skill from the physical initialization. The mean skill for the entire month of October, 1991 is around 0.85. The mean one day forecast skill for

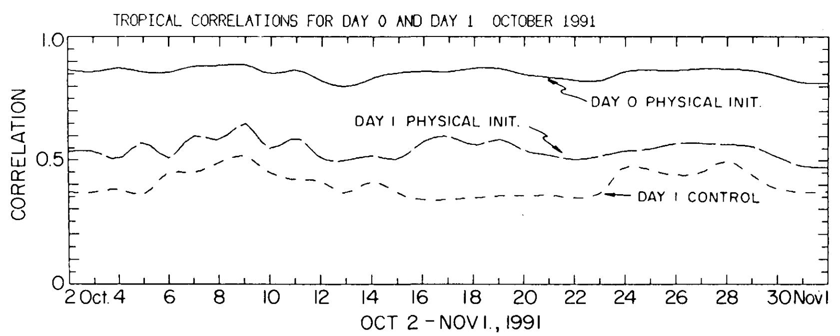

Fig. 2. Absolute correlation of "observed", based on FSU rainfall analyses and the predicted rainfall. Top line is for the day 0 skill with physical initialization, the middle (long dashed) line shows the day 1 skill with physical initialization and the bottom (short dashed) line shows the day 1 skill based on the control run without physical initialization. Abscissa shows days of the month.

the physically initialized experiment is around 0.55. The mean skill of the one day forecast of the control run (without physical initialization) is around 0.40. The one day skill with the physical initialization far exceeds the skill of operational forecasts which are of the order of 0.20–0.40. This demonstrates a major improvement in the one day rainfall forecast over the global tropics from physical initialization.

6. On the performance of the operational NMC and ECMWF models

During late 1991, as a result of the NMC operational global modeling effort (Kanamitsu et al., 1991) the spectral statistical interpolation (SSI) was introduced. This new analysis scheme uses temperature and specific humidity observations rather than height and relative humidity observations since these variables are closer to the forecast variables used in the NMC global spectral model (Parrish and Derber, 1992a). The current version of the SSI uses 100 iterations for both the moisture analysis and the dynamic variables. The moisture analysis is completely independent from the analysis of the other variables. SSI had lead to a major improvement of the operational forecasts, according to Parrish and Derber (1992b) and Kalnay et al. (1991). The NMC global data assimilation system (GDAS) provides 6-hourly rainfall accumulations of convective and large-scale precipitation. This study will focus solely upon the tropics.

An effort was recently made by NMC to study the impact of physical initialization on parallel (non-operational runs), Mathur et al. (1992). In that effort a strong positive impact on tropical prediction from the inclusion of a reverse cumulus parameterization within the 6-hourly assimilation cycle was demonstrated. The operational model does not include this feature at the present time.

The ECMWF data assimilation system consists of a multivariate optimal interpolation analysis, a non-linear normal mode initialization and a high resolution global spectral model which produces a first-guess forecast for the subsequent analysis with data being assimilated every six hours. At the time of the experiments, October, 1991, the model resolution had just been increased to triangular truncation at 213 waves (T213) on 31 vertical levels (ECMWF, 1993).

A comparison of day 0 rainfall from the post physical initialization procedure and the NMC GDAS to the FSU rainfall analysis is shown in Fig. 6a. The ECMWF precipitation fields archived as analysis data were not available due to a lack of confidence in the validity. Ongoing research at that center is aimed at providing improved precipitation analyses as stated in ECMWF, 1993.

The absolute correlation coefficient comparisons shown here were calculated using the total rainfall as combined to cover the corresponding 24-h period. These comparisons are for day 0 and day 1 only.

The day 0 correlations imply that the physical initialization procedure yields a very realistic rainfall. The correlation coefficients for the period are substantially higher than those the NMC GDAS rainfall provides when compared to the FSU rainfall analyses. This large difference can be attributed to two main contributors for this lower measure of skill. The NMC GDAS is producing rainfall analyses which do not seem to be directly coupled to the dynamics of the initial state of the model forecast. When viewing the GDAS rainfall, it is easy to see that the tropical oceanic precipitation is smaller scale and not well organized. Also, there seems to be an abundance of orographically induced precipitation. The monthly accumulation of rainfall for this period (i.e., summing the GDAS precipitation for all of October, 1991) exhibits some values exceeding 1000 mm/month which seems to be excessive.

Fig. 6b illustrates the absolute correlations of various one day forecast rainfall to the verification which is the FSU analysis. The post physical initialization forecast exhibits the highest correlation coefficients. This is seen uniformly throughout the experiment period. The control and ECMWF forecast are very similar. This similarity is not very surprising since the FSU physical initialization and FSU control forecasts used the ECMWF III-B analyses as the initial state for the model. A reason for the discrepancy is that the ECMWF model is at the horizontal resolution T213 while the FSU model is at the resolution T106. The ECMWF forecast may be unfairly penalized because the FSU rainfall analysis is of lower resolution.

The NMC forecast rainfall shows a skill which is much less than the other members of the group, however, the small-scale nature of the precipitation may be correctly predicted but the FSU analysis does not exhibit the same amount of small-scale variability.

Table 3 capsulizes the absolute correlations into an ensemble mean for each member of the comparison. The important information that the physical initialization procedure builds into the initial state for the forecast not only provides an improved rainfall analysis (nowcast), but allows for a substantially higher correlation at day 1 which noticeably surpasses not only the FSU control forecast but the operational centers which were examined. This comparison is valid for only October 1991 and it is felt that a regional comparison would likely yield different results, however, the skill of rainfall prediction via the use of physical initialization has a marked impact from a global tropics perspective. It is important to note that the 1-day forecast skill of persistence was around 0.30 which implies that the physically initialized case has much more skill than the control case, but the control case is still a skillful forecast compared to persistence. This allows for a more clear understanding of how much improvement is seen by the physical initialization procedure.

Table 3. *Mean absolute correlation of daily rainfall over the tropics for October 1991*

	Correlation
FSU rain versus FSU (physical initialization) ensemble day 0	0.85
FSU rain versus NMC forecast ensemble day 0	0.26
FSU rain versus FSU (physical initialization) ensemble day 1	0.55
FSU rain versus FSU control (no physical initialization) ensemble day 1	0.40
FSU rain versus ECMWF forecast ensemble day 1	0.35
Persistence error of day 1 forecast	0.31
FSU rain versus NMC forecast ensemble day 1	0.20

7. Monthly mean rainfall

Since the physical initialization forces the analysis of the daily rain towards the observed amount to an accuracy of nearly 85% (i.e., correlation of 0.85), it is not surprising that one can attain a rather high skill for the monthly total rainfall by simply adding a month of daily observations. The "observed" and predicted monthly total rainfall for October, 1991 are shown in Figs. 3a and 3b. There is a very good agreement between the details in both of these analyzed fields. The results over the global tropical belt between 29.719S and 29.719N are shown. Even smaller scale features of the rainfall maxima over most regions have been reproduced by the proposed initialization.

The proposed physical initialization was only invoked over the tropics, i.e., approximately 30S to 30N. In Fig. 3 we note a lack of agreement between the "observed" and the physically initialized monthly rainfall over the South Pacific Convergence Zone east of Australia. That region of discrepancy is due to the 29.719S boundary for the physical initialization. It shows that convective rain was occurring along the SPCZ near 30S and the model was not able to recover it because of interaction with midlatitude systems which were not physically initialized due to the latitudinal cut off. This perhaps calls for the need of an extension of the boundaries of the physical initialization beyond the tropics.

In Fig. 4, we show the difference between the predicted and the observed monthly mean values (expressed in the units of mm/day). The difference between the observed and the predicted fields are less than ± 2 mm/day over most regions. The maximum difference over some isolated points is of the order of ± 6 mm/day. The largest discrepancies are noted over Brazil, Africa and over the maritime continent (near Indonesia). The discrepancy at the SPCZ near 30S has already been addressed.

The coverage of the SSM/I instrument may be one reason why the discrepancies arise. The areas where the maximum differences occur are the areas which have the highest total rainfall for October, 1991. This can be seen in the Global Precipitation Climatology Project (GPCP) precipitation estimates of monthly accumulated rainfall. These estimates are computed using techniques developed by Arkin (1979), Arkin and Meisner (1987) and Janowiak and Arkin (1991) which combine many

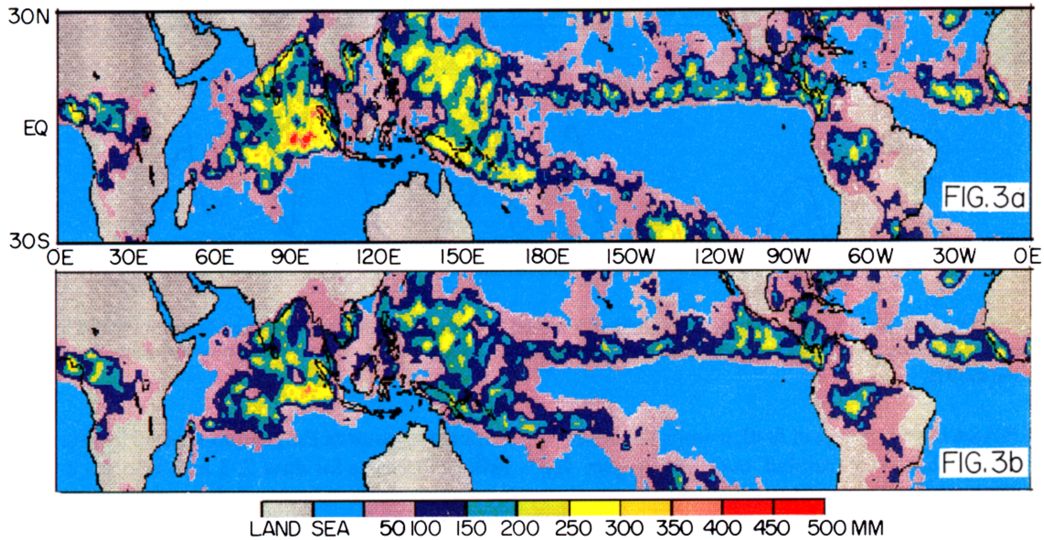

Fig. 3. Total rainfall for October, 1991. (a) "observed" via FSU analyses, (b) physical initialization at day 0, units are mm/month.

satellite products to produce a rainfall analysis. It appears that the SSM/I experiences small data voids between the satellite swaths. These data voids are virtually nonexistent when two satellites are providing observations; however, for this time period the DMSP F10 satellite SSM/I was not providing a steady stream of data, and the 85 GHz channels were faulty on the DMSP F8 satellite.

In a region not covered by SSM/I, the OLR sharpened rainfall (Gairala and Krishnamurti, 1992) will be a close approximation but will be lacking in the higher intensities which the SSM/I instrument observations provide. These discrepancies may not be entirely related to SSM/I observations, since the land area rain is largely controlled by the model assimilation history. This problem could be related to sparsity of raingauge stations over Africa.

This is a first attempt to demonstrate the possibility of obtaining a very good agreement between "observed" and assimilated monthly mean rainfall. We should, however, note that the assimilation can be only as good as the observations of rain provided to it. With the possibility of improved rainrate measurements from TRMM (Tropical Rainfall Measurement Mission

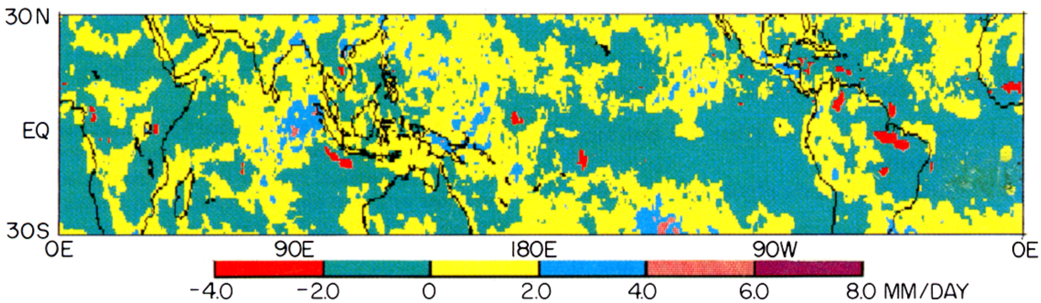

Fig. 4. Daily mean difference between the "observed" and physically initialized day 0 seen in Figs. 3a, b, (mm/day).

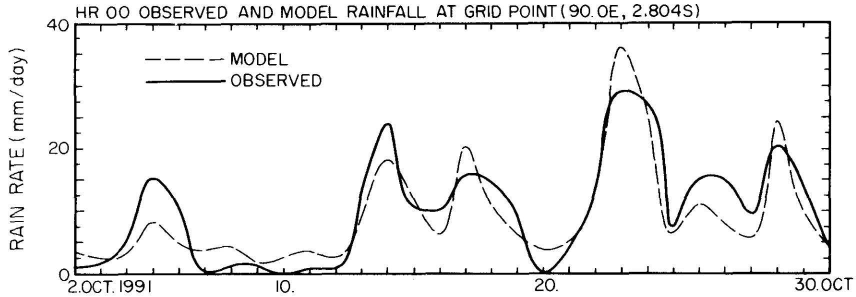

Fig. 5. The time history of the physically initialized (dashed line) rainrate and the "observed" rainrate (solid line) at a single transform point at forecast hour 0 during the month of October 1991, units are mm/day. Abscissa shows days of the month.

of NASA), we can expect further improvements in the assimilation of rainfall over the tropics for climate studies.

An example of what the reverse similarity accepts and what the model returns for a single transform point, for an entire month, is shown in Fig. 5. The solid line is the rainrate at the end of the physical initialization as "observed" from our analysis, and the dashed line shows what rainrate the model provides. This type of behavior is typical at high rainfall transform grid points. This is an illustration of the nowcasting skill. The observed measures over this area come from a mix of OLR, raingauge and the SSM/I data within that square. The time step of the spectral model (for the semi-implicit time differencing) is 7.5 min. Thus the rainfall data being compared is spatially and temporally averaged over roughly 100×100 km^2 and 7.5 min. The study does not address the time variability of rainfall at a single measurement site.

8. Forecast skill beyond 1 day

Only a limited number of forecasts were executed beyond day 1. We show a typical example in Fig. 7 of the FSU forecast skill for 2 sets of experiments:

(a) control experiment (that did not include physical initialization);

(b) Forecast based on physical initialization.

The skills for days 0 and 1 for the physical initialization are of the order of 0.85 and 0.55 respectively. The day 1 skill with physical initialization is much higher than the control; note there was no rainfall for the control at day 0. This is an important result of the present study. However, the skill of forecasts for days 2, 3 and 4 do not exhibit any appreciable advantage from the inclusion of physical initialization. Physical initialization does not substantially modify the rotational part of the wind. The data void tropical oceans have a poor description of the basic flow field on the synoptic and the mesoscale thus we are not able to enhance the forecast skill beyond the control experiment. The 2, 3 and 4 day skills shown in Fig. 7 are comparable to the day 0 and day 1 skill of operational forecasts (see Fig. 6b).

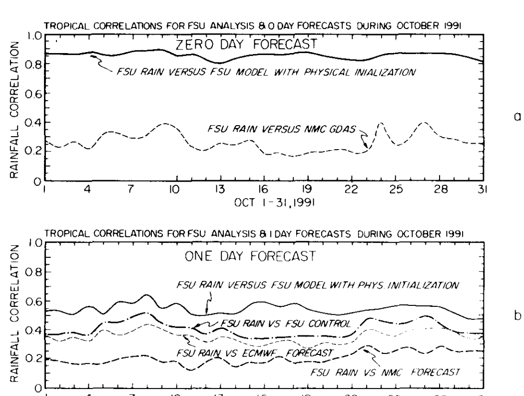

Fig. 6. Absolute correlations of the FSU rainfall analysis at day 0 and day 1 with experiments and the NMC and ECMWF operational centers. (a) FSU rainfall analysis correlated with post-physical initialization rainfall (solid line) and the NMC global data assimilation system rainfall (dashed line); (b) FSU rainfall analysis correlated with the day 1 forecast of FSU post-physical initialization (solid line), FSU control (dot-dashed line), ECMWF model (small dashed line) and NMC model (large dashed line). Abscissa shows days of the month.

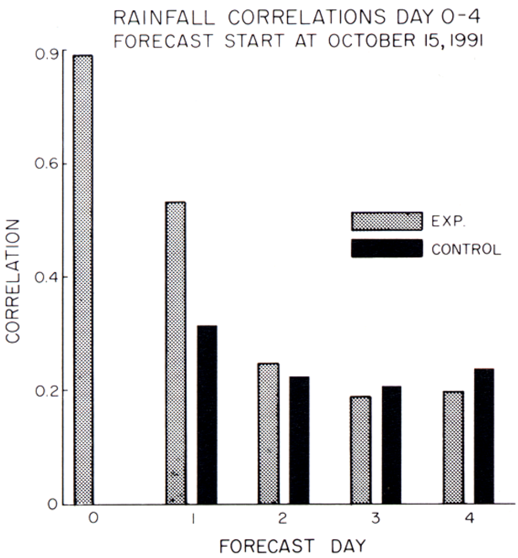

Fig. 7. Correlation of "observed" versus predicted rainfall from the FSU global model for days 0, 1, 2, 3 and 4 of forecast. Light shading shows results for the experiment with physical initialization; dark vertical bars show results for the control experiment which does not include physical initialization.

Another factor that leads to a loss of skill by day 2 is the phase speed errors of the tropical disturbances. Although the storms are very well retained later in the forecast (see Figs. 9 and 10), the slight phase errors in the storm motion result in an effective doubling of the penalty within the rainfall forecast absolute correlations. The "observed" and the predicted rainfall maxima are sufficiently separated and large errors occur over the respective locations. Reduction of such errors will require a better control on the phase speed error of the disturbances. To some extent that can be achieved from a further increase of resolution of the global model. However, the sparsity of overall tropical observations may place a limit on the reduction of such errors.

9. A comparison of the Kummerow and Olson rainfall algorithms

Sample rainrate descriptions for 6 September 1987 for the Kummerow and the Olson rainrate algorithms are illustrated in Figs. 8a and 8b, respectively. This example pertains to a triple typhoon event over the western Pacifc Ocean

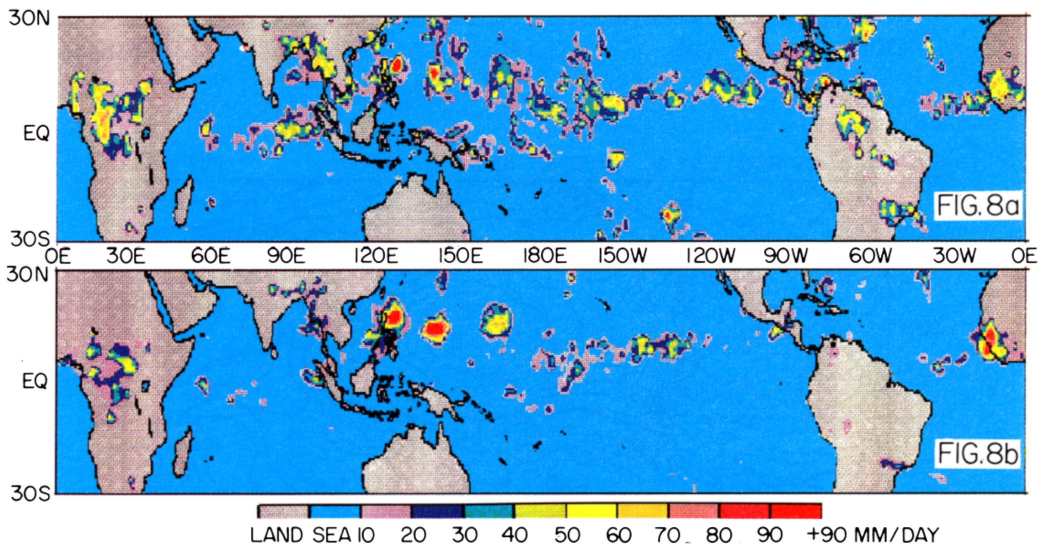

Fig. 8. Physically initialized mean rainrate between 6 September 1987, 600 UTC and 6 September 1987, 12 UTC for two rainrate algorithms. (a) Kummerow and Giglio, (b) Olson.

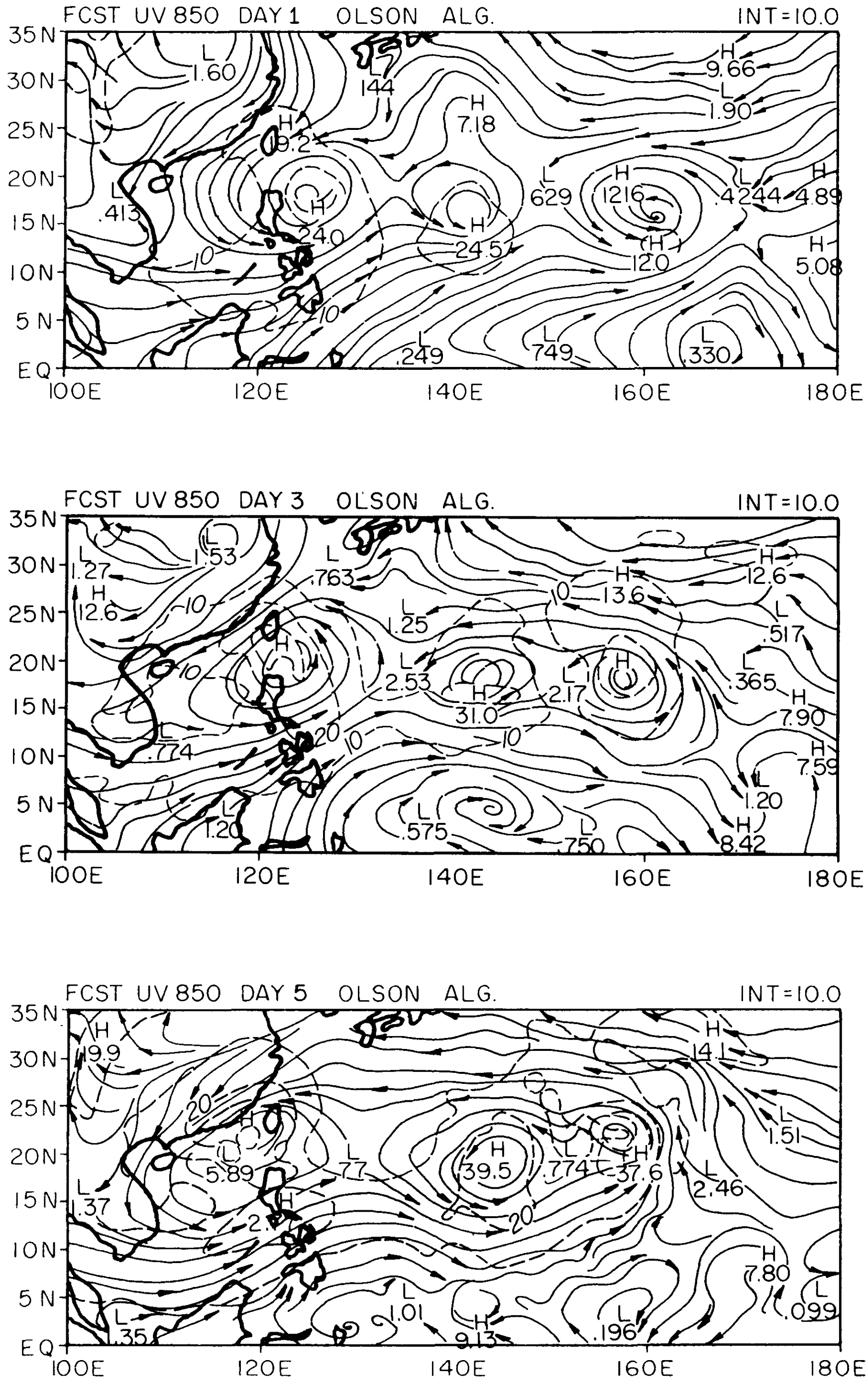

Fig. 9. Predicted 850 mb flow fields at the end of (a) day 1, (b) day 3 and (c) day 5 of forecast for the case which was physically initialized with the Olson algorithm. Solid lines streamlines; dashed lines isotachs (ms^{-1}).

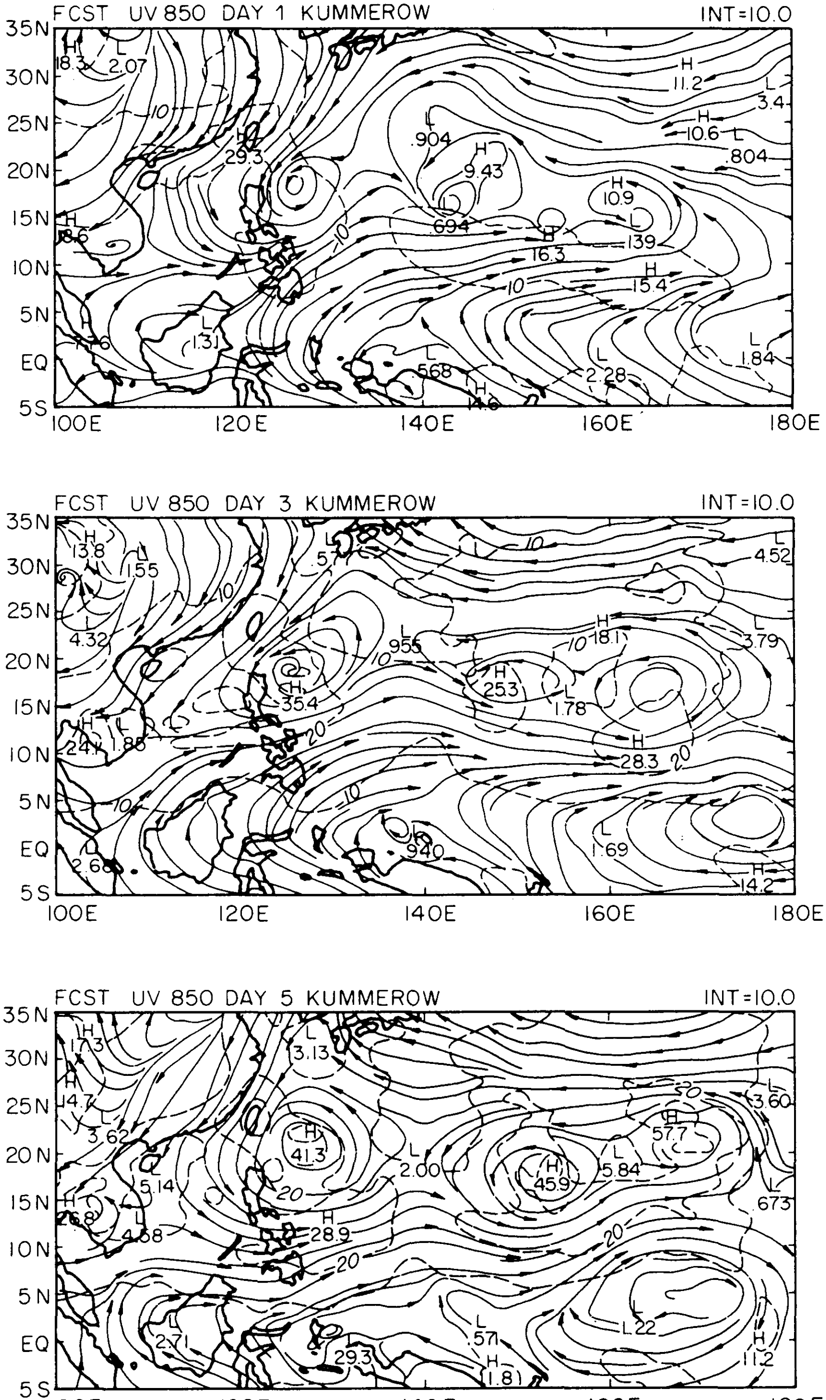

Fig. 10. Same as Fig. 9 except for the Kummerow–Giglio algorithm.

described by Krishnamurti et al. (1993). The color scale identifies the rainfall in the units of mm/day. This comparison suggests that the Kummerow rainrates are somewhat higher than those from the Olson algorithm. The three typhoons are reasonably represented by both algorithms. The African monsoon rainfall appears to be stronger for the Olson algorithm.

We have shown the increase in absolute correlation of the rainfall during the physical initialization period from the use of the two algorithms in Table 4. This table illustrates the absolute correlation of the rainfall over the entire tropical belt between approximately 30°S and 30°N and for the western Pacific triple typhoon region bounded between 5°S to 30°N and 100°E to 180°. The entries along the vertical column represent the correlation between the "observed" and the assimilated rainfall for the respective rainrate algorithms. It is apparent that the final correlation obtained is higher for the Olson algorithm as compared to the Kummerow algorithm.

The reason for this difference lies in part to the equilibration level of rainfall for the T106 resolution of our global spectral model. During a 10-day forecast, the T106 version of the FSU model acquires an equilibration for evaporation (E) and precipitation (P) at a level of roughly 4.35 mm/day. If the assimilation for a particular algorithm yields values of P far different from this equilibration level then the model has difficulties adjusting during and after the physical initialization. The Kummerow algorithm produces an unusually large mean value ($\approx$8.5 mm/day) for the tropicals, whereas the Olson algorithm has a value ($\approx$4.2 mm/day) somewhat closer to the equilibration value for the T106 version of our model. The Pacific typhoon belt experiences an unusually high value of wide spread rain from the Kummerow algorithm, seen in Table 4. It appears from this analysis that care should be exercised in the development of rainrate algorithms to assure that global rainfall rates are reasonable from the global hydrological perspective.

Table 4. *Absolute correlations of rainfall during physical initialization*

Global tropical belt (30°S to 30°N)		
Olson rain in analysis		$\approx$4.20 mm/day
Kummerow rain in analysis		$\approx$8.50 mm/day
Hour	Olson	Kummerow
−18	0.71	0.67
−12	0.82	0.77
−6	0.85	0.77
0	0.85	0.75

Pacific typhoon belt (5°S to 30°N, 100°E to 180°)		
Olson rain in analysis		$\approx$ 9.00 mm/day
Kummerow rain in analysis		$\approx$15.00 mm/day
Hour	Olson	Kummerow
−18	0.80	0.72
−12	0.92	0.81
−6	0.91	0.80
0	0.91	0.80

It should also be noted that the physical initialization does seem to nearly accept whatever rainrates we have been able to provide to it. Thus the initialization is a strong function of the rainrate algorithms which the model is being forced to adjust toward via these reverse algorithms. This brings up the need for a more reliable global distribution of rainrates; hopefully the TRMM would provide us with this information.

9.1. *Comparison of prediction using the Olson and the Kummerow algorithms*

The triple typhoon event was subjected to physical initialization using the Olson and the Kummerow rainrate algorithms. Separate prediction experiments were carried out with these respective algorithms at the horizontal resolution T106. The starting date for these experiments was 5 September 1987 at 12UTC. The experiment based on the Olson algorithm is described in some detail in Krishnamurti et al. (1993). The predicted flow fields at the 850 mb surface for days 1, 3 and 5 of the 2 forecasts are shown in Figs. 9 and 10. The 3 typhoons over the western Pacific ocean (from west to east) are Gerald, Freda and Holly. Holly had become a supertyphoon by September 8th and essentially moved northwards. Gerald moved northwestwards whereas the central storm Freda slowly westward during the first three days.

Overall the track forecasts were handled better with the initialization based on the Olson algorithm. The excessive rain from the use of the Kummerow algorithm was noted over the entire central Pacific ocean. The central and the easternmost typhoons were nearly quasistationary. For both of the rainrate specifications the storms were maintained during the forecasts (which were carried out through 5 days). In contrast, a control experiment where no physical initialization was invoked the storms weakened considerably and Freda and Holly dissipated by day 2 of the forecast, Krishnamurti et al. (1993). Overall both forecasts with the rainrate initialization appear quite impressive when compared to the control forecast.

9.2. *Predicted rainrates from the use of the Olson and Kummerow algorithm*

We shall present the different 24-h rainfall accumulations from the experiments and compare those to an analysis of rainfall which is valid on day 2 of the forecast. The 4 panels of Fig. 11 illustrate these different forecasts in mm/day.

Fig. 11a shows the results of the control experiment where no physical initialization was invoked. What is conspicuous is the absence of heavy rain-

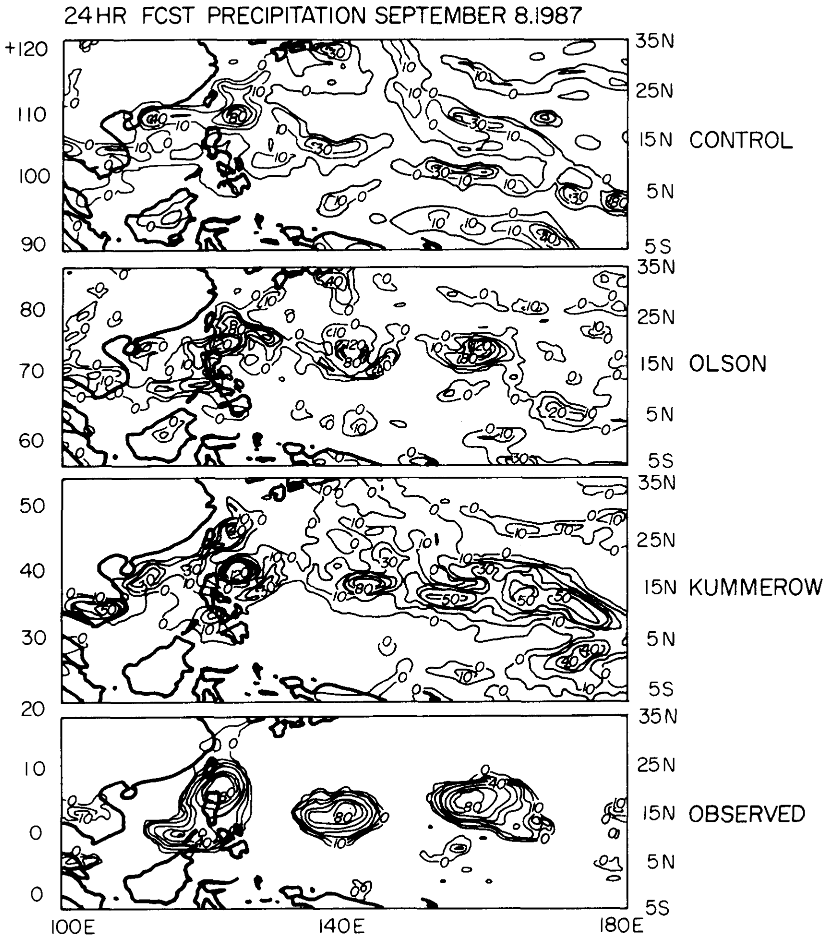

Fig. 11. Forecast 24-h accumulated rainfall totals for day 1 to day 2 for (a) the control experiment, (b) forecast physically initialized using the Olson algorithm, (c) forecast physically initialized using the Kummerow algorithm and (d) FSU analysis "observed" rainfall based on OLR, raingauge and SSM/I via Olson algorithm. Units are mm/day. Color bar shown on left.

fall maxima for the central and the easternmost typhoons Freda and Holly. These storms had essentially dissipated by day 2 of the forecast in the control run. The forecast of rain initialized with the Olson algorithm is shown in Fig. 11b. Intense rainfall rates exceeding 110 mm/day were predicted for all three storms. The phase errors appear to be quite small; this can be inferred from Fig. 11d, where the "observed" rainfall based on OLR, SSM/I via the Olson algorithm and raingauge are displayed (at the resolution of the T106 transform grid which is of the order of 100×100 square kilometers). The analyzed maximum rainfalls for the three typhoons are around 85 mm/day. Fig. 11c shows the results of forecasts which were initialized using the Kummerow algorithm. Although rainfall maxima are evident for all 3 storms, widespread rainfall is predicted in this experiment. The westernmost storm Gerald was predicted very well by both of the rainfall initialization algorithms.

It appears that the Olson algorithm provides a better definition of rainfall for the three typhoons, the Kummerow algorithm, used in this context, appears to provide a somewhat excessive spread of rain. However, when comparing the results with the control it is evident that physical initialization appears to aid in the retention of the storms during these forecasts (Krishnamurti et al., 1993).

10. Concluding remarks

In this study, we have explored the impact of physical initialization on tropical rainfall assimilation and forecasts. We have looked at two different microwave-based rainrate algorithms for the definition of the tropical rainfall. Introduction of a mix of measurements from OLR, SSM/I and raingauges within a physical initialization scheme has improved the nowcasting and the one day forecasting skill substantially.

Using a large, month long, sample of assimilation-prediction experiments a correlation of roughly 0.85 for the mean nowcasting skill of rainfall was demonstrated in this study. The observed and the predicted rain are averages over the transform grid squares of a global model which was run at a horizontal resolution of T106 (i.e., transform grid separation of roughly $100 \times 100\ \mathrm{km}^2$ in the tropics). The mean correlation for day 1 of the forecast is around 0.55 and exceeds the current operational capability. However as one proceeds beyond day 1 the skill falls off rapidly towards the operational levels. This loss of skill beyond day 1 is attributed to a lack of adequate observations to define the rotational part of the wind on synoptic and subsynoptic scales. The physical initialization does enhance the divergent part of wind consistent with the rainfall description.

Another possible factor for the loss of skill (measured by absolute correlation of rainfall at transform grid squares) may arise from small phase errors in the forecast of tropical disturbances. Although heavy rain is predicted by this procedure the phase errors in the position of typhoons appear to contribute to substantial root mean square errors of the rainfall.

Physical initialization using two different rainrate algorithms illustrates different amounts of tropical rain, one being systematically higher than the other. Physical initialization appears to accept these different analyses of rainrates and modifies the pre-existing description of the initial state. Thus we are led to conclude that physical initialization can only be as accurate as the rainfall provided to it. This brings up the need for better measurements of tropical rainfall, that is a goal of a future satellite radar-microwave mission called TRMM.

The current global model invokes a modified version of the Kuo scheme for the cumulus parameterization, Krishnamurti et al. (1993). The vertical distribution of heating implied by the cumulus parameterization needs to be compared with observations. Estimation of the vertical distribution of heating is also a goal of the proposed TRMM program. Hopefully the research on physical initialization could be steered to exploit these data sets and improve the overall rainfall forecasts over the tropics beyond the short-range.

The resolution of the present study, T106, does not permit us to examine meso-convective disturbances. We are currently extending the physical initialization to very high resolution global models such as T213. Even at this resolution the meso-convective disturbances whose scales are of the order of a few hundred kilometers are barely resolved. The resolution of the SSM/I microwave channels varies from roughly 30 to 60 kilometers. Physical initialization at a high resolution is able to nearly reproduce the "observed" rainrate over the transform grid squares and modifies the vertical structure of humidity and in the evolution of stronger divergence (and possibly of smaller scale motions) and heating fields locally. Lacking mesoscale data we must rely on the physical initialization to generate the structure of the mesoconvective systems. This shall be one of the major efforts for numerical weather prediction in the future.

11. Acknowledgements

Financial support for this work was received from NSF grant ATM 8812053, NASA grant NAG 5-1595, ONR grant N 00014-93-1-0243, and NASA grant NAG 8-914. Computations for this work were carried out on the National Center for Atmospheric Research (NCAR) supercomputer CRAY/YMP 8/64; NCAR is sponsored by the National Science Foundation.

REFERENCES

Arkin, P. A. and Meisner, B. N. 1987. The relationship between large-scale convective rainfall and cold cloud over the Western Hemisphere during 1982–84. *Mon. Wea. Rev.* **115**, 51–74.

Arkin, P. A. 1979. The relationship between the fractional coverage of high cloud and rainfall accumulations during GATE over the B-scale array. *Mon. Wea. Rev.* **107**, 1382–1387.

Businger, J. A., Wyngard, J. C., Izumi, Y. and Bradley, E. F. 1971. Flux profile relationship in the atmospheric surface layer. *J. Atmos. Sci.* **28**, 181–189.

Chang, C. B. 1979. *On the influence of solar radiation on diurnal variation of surface temperatures on African disturbances.* Rep. No. 79-3, Dept. of Meteor., The Florida State University, 157 pp.

European Centre for Medium-range Weather Forecasts, 1993. The description of the ECMWF/WCRP Level III, A global atmospheric data archive. *Technical attachment*, 49 pp.

Gairola, R. K. and Krishnamurti, T. N. 1992. Rain rates based on SSM/I, OLR and raingauge data sets. *J. Meteorol. Atmos. Phys.* **50**, 165–174.

Janowiak, J. E. and Arkin, P. A. 1991. Rainfall variations in the tropics during 1986–89, as estimated from observations of cloud top temperatures. *J. Geophys. Res.* **96** Supl., 3359–3373.

Kalnay, E., Petersen, R., Kanamitsu, M. and Baker, W. E. 1991. U.S. operational numerical weather prediction. *Reviews of Geophysics*, IUGG, 104–114.

Kanamitsu, M., Alpert, J. C., Campana, K. A., Caplan, P. M., Deavon, G. G., Iredell, M., Katz, B., Pan, H.-L., Sela, J. and White, G. H. 1991. Recent changes implemented into the global forecast system at NMC. *Weather and Forecasting* **4**, 425–435.

Kanamitsu, M., Tada, K., Kudo, K., Sato, N. and Isa, S. 1983. Description of the JMA operational spectral model. *J. Met. Soc. Japan* **61**, 812–828.

Kanamitsu, M. 1975. *On numerical prediction over a global tropical belt.* Report No. 75-1, Dept. of Meteorology, Florida State University, Tallahassee, Florida 32306, pp. 1–282.

Krishnamurti, T. N., Bedi, H. S. and Ingles, K. 1993. Physical initialization using SSM/I rain rates. *Tellus* **45A**, 247–269.

Krishnamurti, T. N., Xue, J., Bedi, H. S., Ingles, K. and Oosterhof, D. 1991. Physical initialization for numerical weather prediction over the tropics. *Tellus* **43A/B**, 53–81.

Krishnamurti, T. N., Bedi, H. S., Heckley, W. and Ingles, K. 1988. Reduction of the spinup time for evaporation and precipitation in a spectral model. *Mon. Wea. Rev.* **116**, 907–920.

Krishnamurti, T. N., Ingles, K., Cocke, S., Pasch, R. and Kitade, T. 1984. Details of low latitude medium range numerical weather prediction using a global spectral model (II). Effect of orography and physical initialization. *J. Meteor. Soc. Japan* **62**, 613–649.

Krishnamurti, T. N., Low-Nam, S. and Pasch, R. 1983. Cumulus parameterization and rainfall rates (II). *Mon. Wea. Rev.* **111**, 816–828.

Kummerow, C., Mack, R. A. and Hakkarinen, I. M. 1989. A self-consistency approach to improve microwave rainfall estimates from space. *J. App. Meteor.* **28**, 869–884.

Kummerow, C. and Gilio, L. 1994. A passive microwave technique for estimating rainfall and vertical structure information from space. Part 1: Algorithm description. *J. App. Meteor.* **33**, 3–18.

Kuo, H. L. 1965. On formation and intensification of tropical cyclones through latent heat release by cumulus convection. *J. Atmos. Sci.* **22**, 40–63.

Kuo, H. L. 1974. Further studies of the parameterization of the influence of cumulus convection on large scale flow. *J. Atmos. Sci.* **31**, 1232–1240.

Louis, J. F. 1981. A parametric model of vertical eddy fluxes in the atmosphere. *Bound. Layer. Meteor.* **17**, 187–202.

Mathur, M. B., Bedi, H. S., Krishnamurti, T. N., Kanamitsu, M. and Woollen, J. S. 1992. Use of satellite-derived rainfall for improving tropical forecasts. *Research Highlights of the NMC Development Division: 1989–1991.* U.S. Dept. of Commerce/ NOAA/NWS, May 1992, 230–233.

Miller, D. and Fritsch, J. M. 1991. Mesoscale convective complexes in the western Pacific region. *Mon. Wea. Rev.* **119**, 2978–2992.

Olson, W. S., Fontaine, F. S., Smith, W. L. and Achtor, R. H. 1990. *Recommended algorithms for the retrieval of rainfall rates in the tropics using SSM/I (DMSP-F8)*. Manuscript. University of Wisconsin, Madison, 10 pp.

Parrish, D. F. and Derber, J. C. 1992a. The NMC global variational analysis system. *Research Highlights of the NMC Development Division: 1989–1991*. U.S. Dept. of Commerce/NOAA/NWS, May 1992, 173–177.

Parrish, D. F. and Derber, J. C. 1992b. The National Meteorological Center's Spectral Statistical Interpolation analysis system. *Mon. Wea. Rev.* **120**, 1747–1763.

Tiedtke, M. 1984. The sensitivity of the time-mean large-scale flow to cumulus convection in the ECMWF model. *Workshop on Convection in large-scale numerical models.* ECMWF, 28 Nov.–1 Dec. 1983, 297–316.

Wallace, J. M., Tibaldi, S. and Simmons, A. J. 1983. Reduction of systematic forecast errors in the ECMWF model through the introduction of envelope orography. *Quart. J. Roy. Met. Soc.* **109**, 683–718.

Yanai, M., Esbensen, S. and Chu, J. H. 1973. Determination of bulk properties of tropical cloud clusters from large-scale heat and moisture budgets. *J. Atmos. Sci.* **30**, 611–627.